Sargent, P. *et al*. (2020) ***Géotechnique Letters*** **10**, 1–9, https://doi.org/10.1680/jgele.19.00055

Mineralogy and microstructure effects on the stiffness of activated slag treated alluvium

P. SARGENT*, N. H. JABER† and M. ROUAINIA‡

Alkali-activated alumino-silicate-based industrial waste products have recently proven to be beneficial as low-carbon alternatives to ordinary Portland cement binders for strengthening soft soils. This paper examines the small-strain stiffness behaviour of a UK silty alluvial soil in its natural state and artificially cemented using sodium hydroxide-activated ground-granulated blast-furnace slag (GGBS). Undrained triaxial testing with bender element measurements revealed that the initial small strain shear stiffness (G_{max}), shear strength and hydraulic conductivity of the alluvium were all significantly enhanced after 28 d curing. Microstructural and mineralogical analyses were carried out on stabilised soil to understand the mechanisms better through which the enhanced engineering performances were achieved. Through hydration and pozzolanic reactions, a significant proportion of the clay minerals within the original soil had been converted into new cementitious hydrates. These were observed to infill pore spaces, coating soil and GGBS particle surfaces and increased interparticle bonding throughout the matrix of the material. The outcomes from this study have the potential to contribute towards improving current practices for modelling cemented soils and ultimately making geotechnical designs involving deep soil mixing less conservative.

KEYWORDS: microscopy; mineralogy; soil stabilisation

INTRODUCTION

Soft alluvial soils possess low bearing capacities and high compressibilities, presenting difficulties in the design and construction of foundations. Rather than using expensive conventional piling methods, an increasingly popular alternative is deep soil mixing (DSM) ground improvement. The most commonly used DSM binder is ordinary Portland cement (CEM-I), due to its high strength and durability performance (Horpibulsuk *et al*., 2010; Kang *et al*., 2017; Hancock, 2019; Zhu *et al*., 2019). However, its continued use is environmentally unsustainable as its production accounts for ∼7% of global carbon dioxide (CO_2) emissions (Pourakbar *et al*., 2015; Sargent *et al*., 2016). Hence, efforts are now being made to focus on the development of low carbon binders, with an emphasis on improved circular economy by utilising industrial waste products (IWMs).

There have been many unconfined compressive strength (UCS)-based laboratory studies undertaken on soils stabilised with IWMs including GGBS, pulverised fly ash (PFA) and biomass ash as partial replacements to CEM-I (Al-Tabbaa & Evans, 1998; Ahnberg, 2007; Horpibulsuk *et al*., 2010; Ghadir & Ranjbar, 2018). While the results from these studies are positive, more effort is needed on the total replacement of CEM-I if the construction sector intends to make a valuable and timely contribution towards reducing global carbon dioxide emissions. Using GGBS and type-F PFA for soil stabilisation requires alkali activation (Haha *et al*., 2011). Sargent *et al*. (2013) revealed that using sodium hydroxide–sodium silicate ($NaOH–NaSiO_3$) activated GGBS-based binders to stabilise an artificial alluvium (silty sandy clay) produced UCS of 6 MPa after 28 d and durability performances exceeding those of CEM-I stabilised mixtures (3 MPa after 28 d). Cristelo *et al*. (2013) performed a similar study, which focused on the use of sodium hydroxide at various molar concentrations (10–15 molar) to activate type F PFA for stabilising a Portuguese sandy clay. The 28 d UCS values recorded in their study ranged between 2 and 12 MPa, which continued to increase up to approximately 45 MPa after 365 d. More recently, Mohammadinia *et al*. (2019) investigated the use of sodium hydroxide–sodium silicate activated type F PFA and GGBS, rather than CEM-I for stabilising loose sands (sourced from Melbourne, Australia) through DSM. UCS values for alkali-activated PFA–GGBS mixtures surpassed FHWA criterion and were at least comparable for CEM-I mixtures after curing periods of 7, 14 and 28 d and for dosages of 16 and 25%. Interestingly, Mohammadinia *et al*. (2019) established that using a higher proportion of GGBS in the PFA–GGBS binder resulted in higher 28 d UCS values being achieved (15 MPa) that surpassed the performance of CEM-I mixtures (9 MPa).

With the prospect of DSM being increasingly used to form deep foundations, further investigation is recommended regarding the small-strain behaviour of cemented soils (Bonal *et al*., 2012). Further to disagreement between studies undertaken by Cuccovillo & Coop (1997) on calcarenite, Yun & Santamarina (2005) on artificially cemented sand and Hird & Chan (2008) on artificially cemented clay, Trhlikova *et al*. (2012) investigated the structure and G_{max} of a CEM-I stabilised kaolin clay. They established that post-yield, G increased with mean effective stress (p') when compression (structure degradation) rates were low (and vice versa). However, Trhlikova *et al*. (2012) were unable to capture pre-yielding behaviour characterised by constant G

Manuscript received 5 November 2019; first decision 18 March 2020; accepted 19 March 2020.
*School of Computing, Engineering and Digital Technologies, Teesside University, Middlesbrough, UK (Orcid:0000-0001-5789-1076).
†Civil Engineering Department, College of Engineering, University of Kerbala, Kerbala, Iraq.
‡School of Engineering, Newcastle University, Newcastle upon Tyne, UK (Orcid:0000-0001-5623-4314).

with increasing p', which is typical of high-strength cemented soils. Rios *et al.* (2014) investigated the small-strain behaviour of artificially CEM-I-treated Porto sand using triaxial apparatus. While failure envelopes were successfully identified for the material in multiple stress planes, Rios *et al.* (2014) were unable to capture strain behaviour sub-0·001% shear strain (ε_q) due to the resolution of strain measurement apparatus used. Rios *et al.* (2017) performed another triaxial-based study on a silty sand stabilised with alkali-activated fly ash, to assess their small-to-large strain behaviour after 28 and 90 d curing. They observed that the strength development behaviour of alkali-activated PFA-stabilised soil contrasted with cement-stabilised counterparts, whereby peak strengths for the latter were recorded after 28 d whereas strength development continued for the former – doubling in initial elastic stiffness (E_0) from approximately 2·9 GPa after 28 d to 6·3 GPa after 90 d. Ultrasonic measurements used by Rios *et al.* (2017) to measure G also revealed that Poisson's ratio of samples slightly decreased during the initial days of curing, which then increased after 7 d. This suggested that curing only has an effect on sample strength and stiffness after 7 d curing, which is contrary to the behaviour of soil–cement mixtures.

This paper presents results from an investigation into the degradation of G_{max} for a soft alluvium stabilised with a new sodium hydroxide-activated GGBS binder after 28 d curing and the resulting mineralogical and microstructural modifications.

MATERIALS AND TESTING METHODOLOGIES

Sample preparation

The alluvium was obtained from Lanton (Northumberland, UK), which has previously been classified in terms of its geotechnical index properties by Sargent *et al.* (2016). According to the Unified Soil Classification System (USCS), the alluvium may be characterised as an inorganic silty clay of low-to-medium plasticity (CL). In terms of particle size grading, the soil was found to have a uniformity coefficient of 4·71 and coefficient of curvature of 0·90. To ensure homogeneous stabilised samples were produced in the laboratory, the soil was oven-dried at 100°C for 24 h and milled down to a fine powder (<40 μm). Further to Sargent *et al.* (2016), a GGBS–sodium hydroxide dosage of 7·5% by dry weight (5% GGBS, 2·5% sodium hydroxide) was added to the soil and mixed mechanically for 5 min. The sodium hydroxide used was in pellet form and had a molarity of 39·997 g/mol. Deionised water was then added to achieve a moisture content of 25% (based on the alluvium's in situ moisture content) and mixed for a further 5 min.

According to BS 1377 (BSI, 1990), cylindrical samples 140 mm long × 70 mm diameter were prepared for triaxial testing. In accordance with Cristelo *et al.* (2013), Sargent *et al.* (2016) and Rios *et al.* (2017), stabilised samples were manually compacted in three layers into polyvinyl chloride moulds to achieve a bulk density of 1·9 Mg/m^3 and then wax-sealed for 28 d curing in a temperature and humidity-controlled room (20°C, 55% relative humidity).

Triaxial testing

Isotropically consolidated undrained (ICU) and unconsolidated undrained (UU) triaxial tests were performed on samples according to BS 1377-8 (BSI, 1990). For ICU tests, sample saturation was confirmed by using the Skempton pore-pressure coefficient 'B' test. B values measured for samples ranged between 0·95 and 0·98 – indicating full saturation had been achieved. During ICU tests, coefficients of vertical permeability (k_v) were also measured, whereby at 22°C k_v values for the untreated and 28 d stabilised alluvium were $1{\cdot}41 \times 10^{-8}$ and $4{\cdot}02 \times 10^{-9}$ m/s, respectively. For sample compression, a constant strain rate of 0·001 mm/min was adopted.

Small-strain measurements

For taking shear stiffness measurements of the untreated alluvium at the end of isotropic consolidation and during compression over small to large ε_q, bender elements (installed within the triaxial top cap and base pedestal) were gently pressed into the sample ends by 3–5 mm. Whereas for 28 d cured GGBS–sodium hydroxide stabilised alluvium samples, 5 mm deep slots were manually created by using a Stanley knife. The material removed from the slots was then re-wetted and used as a coupling agent to infill any gaps between the bender element and the sample, ensuring successful transmission of S-waves. To ensure high-quality S-wave signals, at least three S-wave wavelengths were required to pass through samples. Based on Sargent *et al.* (2016), estimations were made for shear wave velocity (V_s) to select a frequency of 20 kHz for generating S-waves. This was sufficiently high to compensate for the near-field effect (Cai *et al.*, 2015). According to Sargent (2015), the time-domain technique was adopted for determining V_s and ultimately G_{max}.

Mineralogy and microstructure

To investigate the microstructure of the alluvium before and after stabilisation, scanning electron microscopy (SEM) and point elemental energy-dispersive X-ray (EDX) analyses were carried out by using a Philips XL30 ESEM-FEG. Qualitative X-ray diffraction (XRD) analyses were also undertaken to study the mineralogy of the untreated and GGBS–sodium hydroxide-treated alluvium. The equipment used was a PANalytical X'Pert Pro MPD, powered by a Philips PW3040/60 X-ray generator and fitted with an X'celerator detector. Samples were subjected to Cu-Kα X-rays, which had a wavelength of 1·5418 Å. Mineral phase identification was enabled through the use of the PANalytical High Score Plus software and the ICDD Powder Diffraction File 2 Database, sets 1–49 (ICDD, 1999).

RESULTS AND DISCUSSION

Strength and stiffness

Table 1 summarises the triaxial conditions, sample dimensions and bender element measurements for untreated and treated samples. During shearing, V_s decreased with ε_q particularly beyond 0·5%. This is likely due to strain localisation and dilation on yielding.

Figure 1 shows the deviatoric stress (q) – ε_q behaviour of ICU and UU tests. Peak q ranged between 2000 and 2580 kPa for ICU tests and 2430–2980 kPa for UU tests. Stabilised samples chiefly exhibited peak strength with post-yield softening behaviour akin to heavily overconsolidated soils and rocks. However, sample UU_5_600 showed hardening behaviour similar to normally consolidated soils. This can be attributed to the confining stress being greater than the quasi-preconsolidation stress (Ahnberg, 2007) or the apparent overconsolidation ratio linked to the Hvorslev equivalent pressure (Trhlikova *et al.*, 2012). Figure 2 shows the G_{max} degradation curves for all ICU and UU tests.

From Fig. 2(a), stabilisation and p' influence G_{max} of ICU samples, whereby higher p' result in higher G_{max}. This is inconsistent with Hird & Chan (2008) and Dvorkin *et al.*

Table 1. Summary of sample testing conditions and G_{max} measurements taken at the start of compression

Material	Triaxial condition	p'_0: kPa	Sample length: mm	Sample diameter: mm	ρ: Mg/m^3	V_s: m/s	G_{max}: MPa
Untreated Lanton alluvium	ICU	50	140·12	71·42	2·05	211·02	89·06
28 d cured 7·5% GGBS–sodium hydroxide-treated Lanton alluvium	ICU	50, 200, 400, 600	139·83–141·30	73·22–73·66	1·98–2·02	743·50–980·43	1052·80–1877·45
	UU	50, 200, 300, 600	138·58–140·20	73·60–74·09	1·97–1·99	833·81–894·65	1082·93–1527·09

NB: sample ID notation 'ICU/UU_sample no._p'_0 condition'.

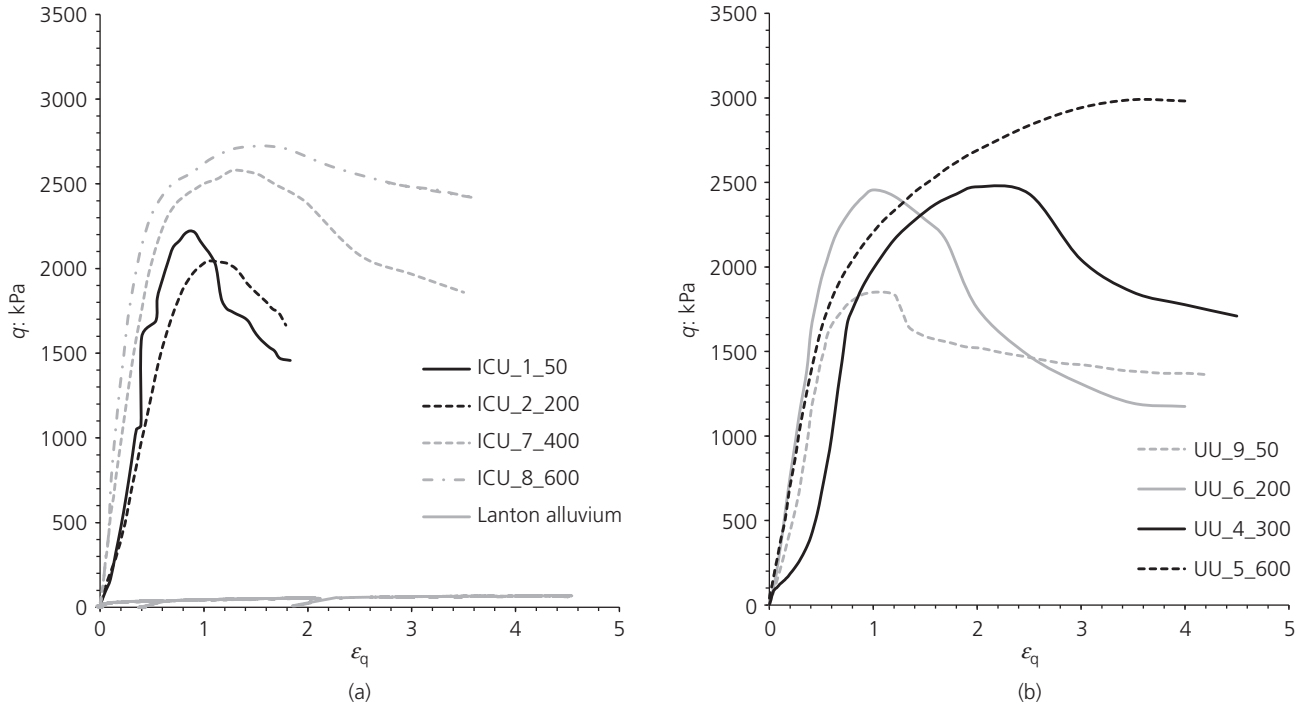

Fig. 1. Deviatoric stress–shear strain response of the untreated and 28 d cured GGBS–sodium hydroxide-treated Lanton alluvium under (a) ICU and (b) UU triaxial testing conditions

(1991). The relationship between p' and G_{max} is dependent on the degree of cementation within the stabilised soil's matrix. For stabilised soils whose matrices are strongly cemented, increasing the p'_0 condition is not anticipated to break down the cementitious bonds, as observed by Consoli *et al.* (2009). Conversely, for stabilised soil matrices with weaker levels of cementation, increasing p' will more likely cause cementitious bonds to collapse – resulting in lower values of G_{max}. Figure 2(b) demonstrates the effect of p' on G_{max} is less significant for UU tests. This corroborates typical behaviour for untreated soils, demonstrating the effect of total against effective stress behaviour. From all the tests undertaken, stabilisation and 28 d curing increased G_{max} of the untreated alluvium by factors of 11–20, achieving 1052–1877 MPa.

Figure 2 shows that the onset of G_{max} degradation for stabilised ICU and UU samples chiefly occurred at $\varepsilon_q = 1\%$. This is a significant improvement compared with the untreated alluvium, where G_{max} degradation started at $\varepsilon_q = 0{\cdot}008\%$. The G_{max} degradation rate for stabilised samples was consistent. However, samples UU_6_200 and ICU_7_400 exhibited different behaviour, whereby their G_{max} started degrading at lower ε_q of 0·36 and 0·1%, respectively. Due to the early onset of G_{max} degradation for these samples, they reached residual G at lower ε_q (0·75% for UU_6_200, 1·7% for ICU_7_400) compared with other samples. This was attributed to the development and propagation of micro-cracks, which may be a result of variability in sample mixing quality.

Mineralogical and microstructural features

Mineralogy.

Untreated alluvium. XRD results for the untreated alluvium are presented in Fig. 3, whereby quartz (Q) was the most dominant mineral phase due to the soil's high sand and silt contents. Albite (Na) and orthoclase (K) feldspars of igneous origin were detected, alongside dolomite (D), chlorite (C) and multiple clay minerals including illite (I), vermiculite (V) and smectite (M).

GGBS–sodium hydroxide-treated alluvium. Similar to the untreated alluvium, XRD spectra for the 28 d stabilised alluvium (Fig. 4) show that quartz was the dominant mineral phase. While XRD was unable to detect cementitious gels (e.g. C–S–H, C–A–H), there are numerous compositional differences in the stabilised alluvium compared with the untreated soil; whereby chlorite, smectite and dolomite minerals could not be detected. It is likely that the calcium

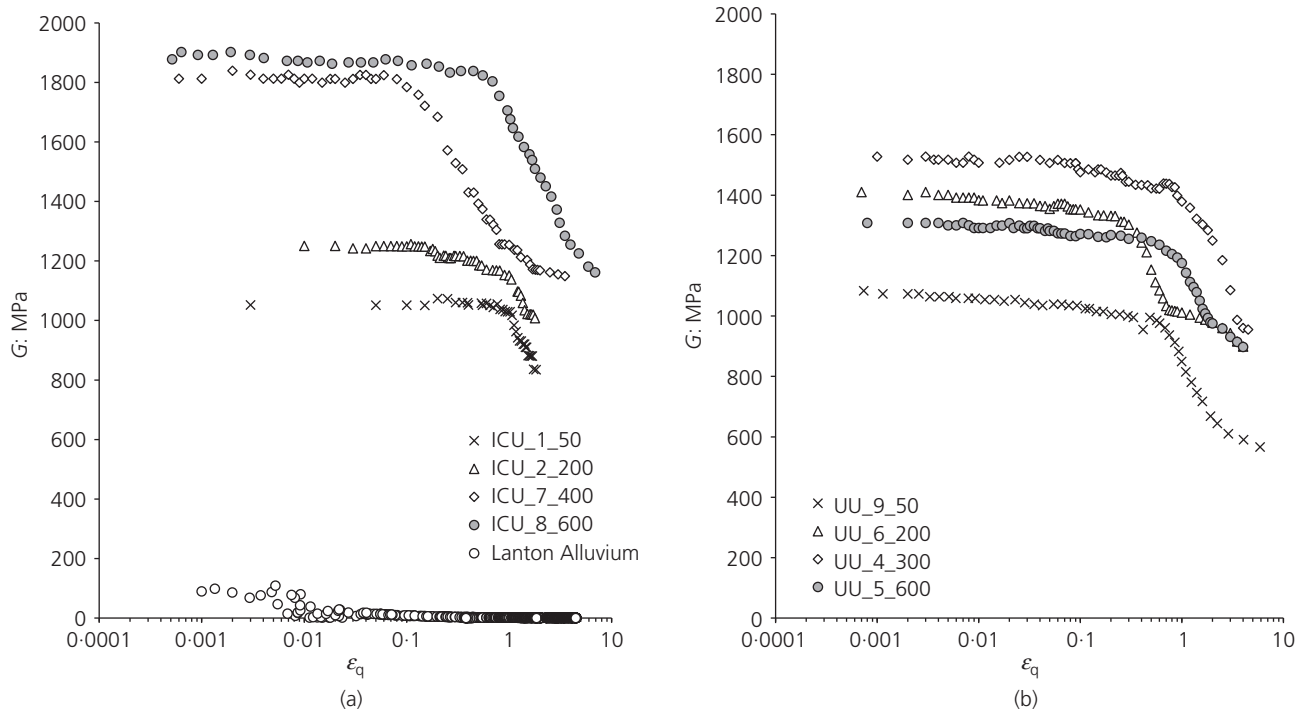

Fig. 2. Small-strain G degradation curves for untreated and 28 d cured Lanton alluvium stabilised with 7·5% GGBS–sodium hydroxide under (a) ICU and (b) UU triaxial testing conditions

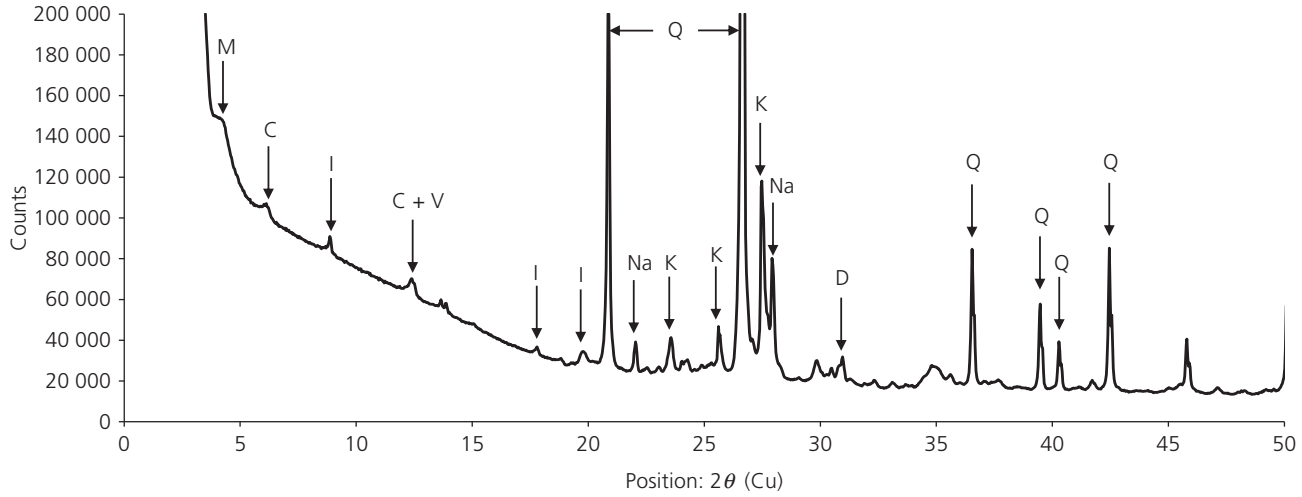

Fig. 3. XRD spectra for untreated Lanton alluvium (includes ICDD interpretation)

content of dolomite, the silica and alumina content of chlorite minerals were utilised during hydration and pozzolanic reactions to form new cementitious gels. The peak intensity for clay minerals within the stabilised alluvium are lower than for the untreated alluvium, indicating that they had partially converted into cementitious gels.

Microstructure.

Untreated alluvium. The SEM micrograph presented in Fig. 5 shows the presence of fine-grained sub-angular sand and silt (quartz) particles, which form inter-particle edge-to-edge and edge-to-face contacts. Illite platelets are widely distributed throughout the soil, occupying pore spaces between silt and sand grains. Smaller chlorite platelets (<10 μm) partially coat surfaces of some larger sand and silt grains. The surfaces of individual particles were clean with no evidence of inter-particle bonding.

EDX spectra (from Fig. 5(a)) are presented in Fig. 6, with the corresponding quantitative elemental composition presented in Table 2. The dominant elemental peaks for silica and oxygen correspond to the soil's high quartz (silt/sand) content. The high potassium and aluminium peaks correspond to the orthoclase feldspar and illite content. The low magnesium content relates to the vermiculite and illite minerals, whereas the calcium peak can be attributed to albite feldspar and the peak for iron is linked with the soil's chlorite content.

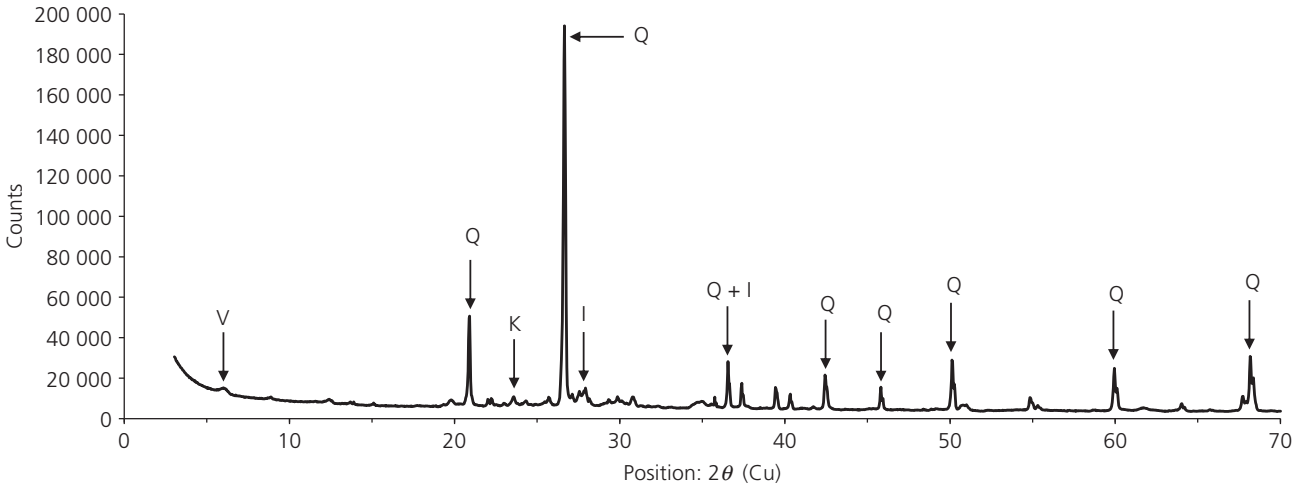

Fig. 4. XRD spectra 7·5% GGBS–sodium hydroxide-treated Lanton alluvium after 28 d curing

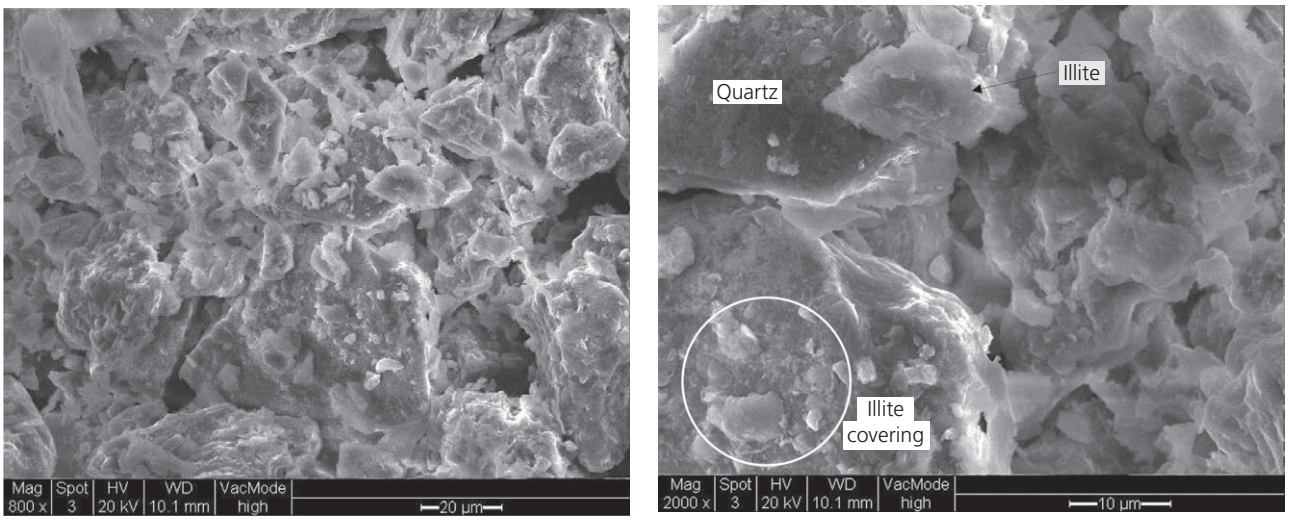

Fig. 5. SEM micrographs of untreated Lanton alluvium at magnifications of: (a) ×800 and (b) ×2000

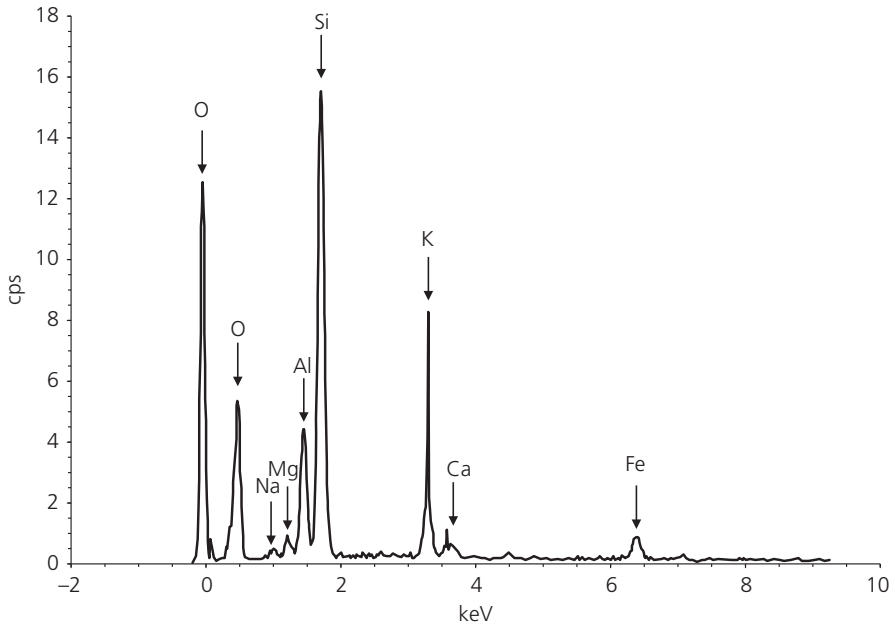

Fig. 6. EDX spectra for Lanton alluvium

GGBS–sodium hydroxide-treated alluvium. Particle morphologies within the treated alluvium (Fig. 7(a)) were more complex compared with the untreated alluvium, due to the inclusion of GGBS and new cementitious growth. GGBS particles were glassy, highly angular and largely < 20 μm, which is attributed to ground granulation in ball mills (Wan *et al*., 2004). EDX spectra for the GGBS are shown in Fig. 8. While GGBS composition varies between iron/steel manufacture plants, the composition of that used in this study is comparable with most GGBS powders with high concentrations of silica, calcium and aluminium, low concentrations of magnesium (Scott *et al*., 1986).

Pore space apertures within the stabilised alluvium were notably smaller compared with the untreated alluvium due to infilling with new cementitious growth, as seen in Fig. 7(a). Soil and sodium hydroxide-activated GGBS particles exhibited face-to-face, edge-to-edge and edge-to-face contacts. This modified microstructure explains the reduced permeability and higher strength of the stabilised alluvium compared with the untreated counterpart.

Features of interest within the material were light-coloured amorphous growth coating sodium hydroxide-activated GGBS particles and bonding them with soil particles, as seen in Fig. 7(b). A significant proportion of amorphous surface coatings were likely to be C–S–H gels; whereby darker inner zones formed during later stages of hydration and lighter outer zones formed during the first few days of hydration (Haha *et al*., 2011).

EDX spectra for the stabilised alluvium are presented in Fig. 9, with the accompanying data in Table 2. The corresponding spectra and data for the amorphous growth in Fig. 7(b) (point '0') are presented in Fig. 10 and Table 3, respectively. While the composition of the alluvium in its untreated and stabilised states were relatively similar, there were some notable differences in Fig. 9 attributable to the GGBS–sodium hydroxide binder and subsequent cementitious reactions. These included larger peaks for sodium, calcium and sulfur.

The EDX results presented in Fig. 10 and Table 3 for point '0' in Fig. 7(b) indicate that the amorphous cementitious growth has high concentrations of silica, aluminium, oxygen and slightly lower concentrations of calcium, sodium, magnesium and iron. This suggests it is likely to be C–(N)–A–H, C–(N)–S–H or C–(N)–A–S–H. The magnesium and iron peaks are likely to be derived from vermiculite and/or chlorite, which have either been partially or entirely converted into cementitious gels. The point elemental EDX spectra for point '1' in Fig. 7(b) were

Table 2. Quantitative elemental composition of Lanton alluvium, GGBS and 28 d cured Lanton + 7·5% GGBS–sodium hydroxide from EDX spectra analysis

Element	Series	Lanton alluvium		GGBS		28 d Lanton + 7·5% GGBS–sodium hydroxide	
		Net	Normally consolidated: wt%	Net	Normally consolidated: wt%	Net	Normally consolidated: wt%
Silicon	K	17 436	31·41	10 695	16·53	13 614	20·28
Aluminium	K	4651	8·39	3582	5·99	3577	5·66
Potassium	K	2888	5·95	703	1·09	1791	3·01
Calcium	K	424	0·92	20 456	36·73	1024	1·80
Sodium	K	186	1·39	210	1·52	178	1·44
Iron	K	1314	5·38	183	0·68	758	2·96
Titanium	K	282	0·75	213	0·55	156	0·34
Sulfur	K	1	0	593	0·99	1	0
Oxygen	K	2245	44·91	1220	32·30	3998	63·78
Magnesium	K	418	0·91	1895	3·72	367	0·72
Total:			100		100		100

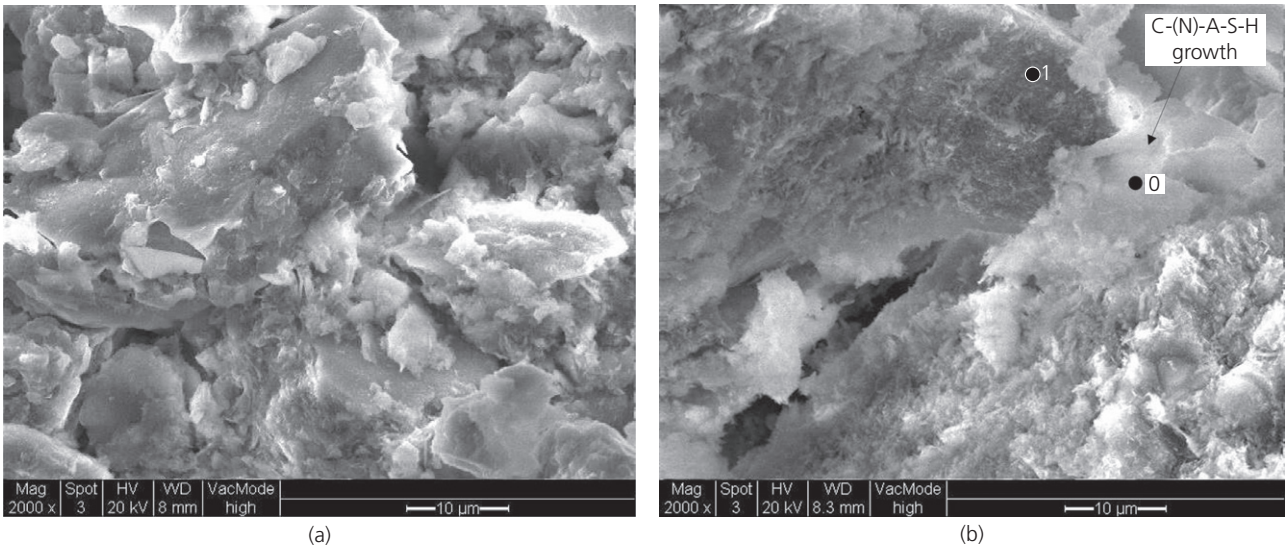

(a) (b)

Fig. 7. SEM micrographs of 28 d cured GGBS–sodium hydroxide-treated Lanton alluvium at ×2000 magnification: (a) small-scale cementitious gel growths and (b) large-scale cementitious gel growths (with locations selected for point elemental EDX analyses)

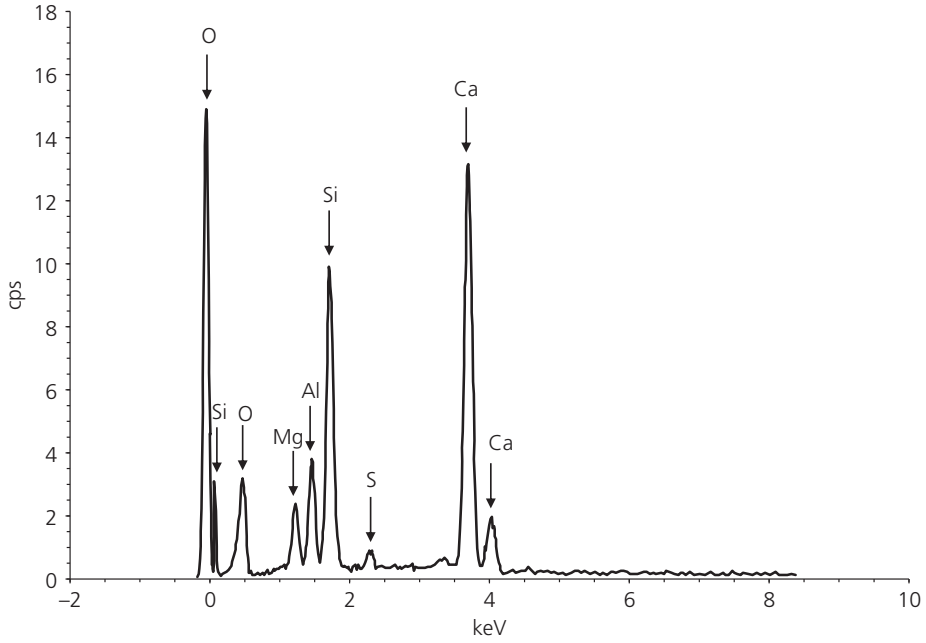

Fig. 8. EDX spectra for GGBS

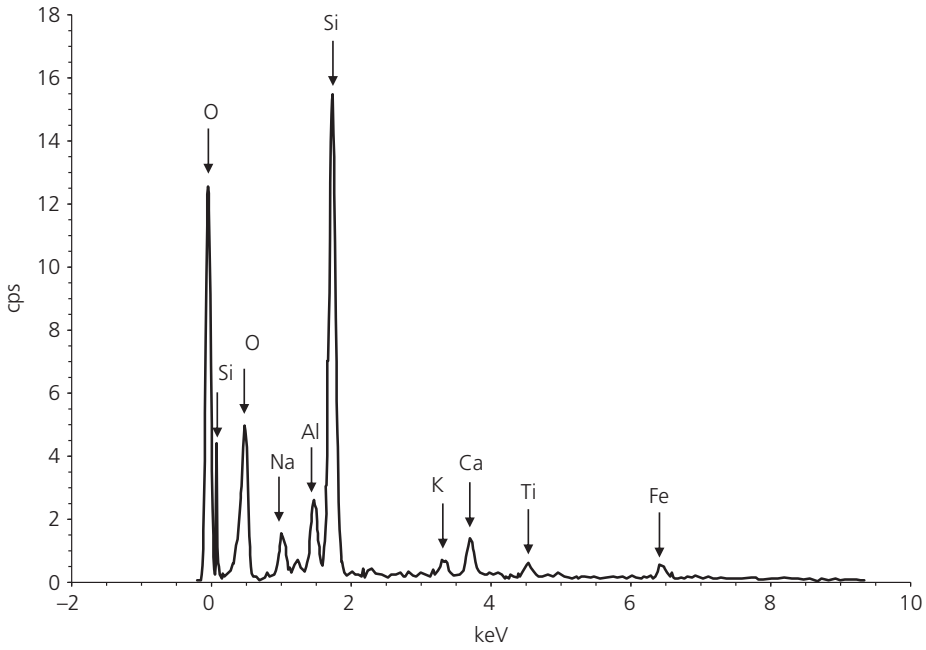

Fig. 9. EDX spectra for 28 d cured GGBS–sodium hydroxide-treated Lanton alluvium (green) compared with spectra for the Lanton alluvium (blue) (based on field of view in Fig. 7(a))

characterised by strong peaks for silica and oxygen, implying the particle was quartz.

No structurally unfavourable Aft minerals were detected within the treated alluvium. Due to the alluvium's low sulfate content (Sargent *et al.*, 2016), this corroborates with Nair & Little (2009), who stated that high moisture and sulfate contents are required for ettringite formation. Furthermore, ettringite was not expected based on hydration kinetics (Haha *et al.*, 2011).

CONCLUSIONS AND RECOMMENDATIONS

Over recent years, there has been heightened interest in the small–to-large strain mechanical behaviour of soft soils stabilised with low carbon binders. This paper has built on this existing body of knowledge by providing insights into the mineralogical and microstructural characteristics of such materials and their influence on mechanical behaviour at the macro scale. An alluvium was stabilised with GGBS–sodium hydroxide at a dosage of 7·5%, which increased G_{max} by up to 20 times reaching values of up to ~1800 MPa after 28 d curing. This treatment also significantly increased the ε_q at which G_{max} started to degrade compared with the untreated soil. XRD analyses indicated that the alluvium experienced mineralogical modifications on stabilisation with GGBS–sodium hydroxide and 28 d of curing. One of the most pertinent changes observed was that some of the clay minerals within the original soil were

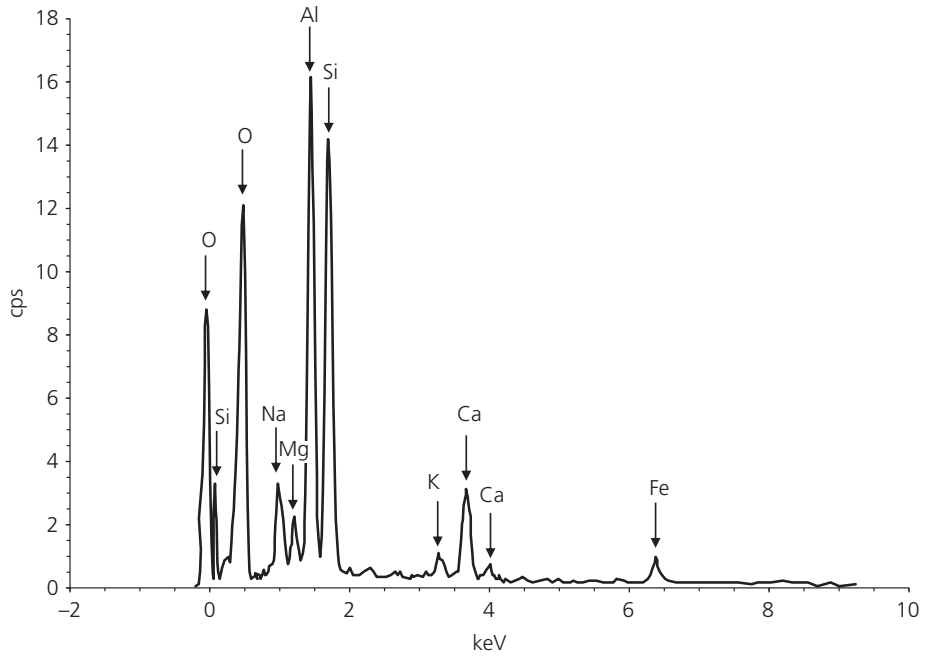

Fig. 10. Point elemental EDX analysis for point '0' shown in Fig. 7(b)

Table 3. Quantitative elemental composition for point '0' shown in Fig. 7(b) from EDX spectra analysis presented in Fig. 10

Element	Series	Net	Normally consolidated: wt%
Silicon	K	17 348	21·49
Aluminium	K	18 358	19·44
Magnesium	K	2148	2·57
Sodium	K	189	0·88
Calcium	K	4419	5·49
Potassium	K	1430	1·70
Iron	K	958	1·89
Oxygen	K	10 457	46·54
Total:			100

partially converted into new amorphous cementitious gels. SEM–EDX analyses indicated that the hydration of GGBS –sodium hydroxide resulted in considerable modifications to the microstructure of the alluvium after 28 d – specifically increased levels of inter-particle bonding due to the formation of C–(N)–A–H, C–(N)–S–H and/or C–(N)–A–S–H. These gels infilled pore spaces throughout the stabilised soil, accounting for its lower permeability and higher strength.

The results published in this study will assist in making a valuable contribution towards developing a better understanding of cemented soil material behaviour in geotechnical design applications, such as DSM foundations and retaining structures. This would enable more sophisticated numerical modelling of cemented soil–structure interactions to be performed, especially where strain tolerances are small (e.g. retaining walls and tunnels). It is also envisaged that such modelling would make geotechnical designs less conservative compared with current industrial practice, where more simplistic constitutive soil models are typically used to model cemented soil behaviour. Further work is recommended to investigate the porous structure of cemented soil materials and their chemical interactions with adjacent natural soils and steel work.

REFERENCES

Ahnberg, H. (2007). On yield stresses and the influence of curing stresses on stress paths and strength measured in triaxial testing of stabilized soils. *Can. Geotech. J.* **44**, No. 1, 54–66, https://doi.org/10.1139/T06-096.

Al-Tabbaa, A. & Evans, C. W. (1998). Pilot in situ auger mixing treatment of a contaminated site – Part 1: treatability study. *Proc. Inst. Civil Engrs, Geotech. Engng* **13**, No. 1, 52–59, https://doi.org/10.1680/igeng.1998.30005.

Bonal, J., Donohue, S. & McNally, C. (2012). Wavelet analysis of bender element signals. *Géotechnique* **62**, No. 3, 243–252, https://doi.org/10.1680/geot.9.P.052.

BSI (1990). BS 1377: Incorporating amendment no. 1, methods of test for soils for civil engineering purposes. London, UK: BSI.

Cai, Y., Dong, Q., Wang, J., Gu, C. & Xu, C. (2015). Measurement of small strain shear modulus of clean and natural sands in saturated condition using bender element test. *Soil Dyn. Earthq. Engng* **76**, 100–110, https://doi.org/10.1016/j.soildyn.2014.12.013.

Cristelo, N., Glendinning, S., Fernandes, L. & Pinto, A. T. (2013). Effects of alkaline-activated fly ash and Portland cement on soft soil stabilisation. *Acta Geotech.* **8**, No. 4, 395–405, https://doi.org/10.1007/s11440-012-0200-9.

Consoli, N. C., Viana da Fonseca, A., Cruz, R. C. & Heineck, K. S. (2009). Fundamental parameters for the stiffness and strength control of artificially cemented sand. *J. Geotech. Geoenviron. Engng* **135**, No. 9, 1347–1353, https://doi.org/10.1061/_ASCE_GT.1943-5606.0000008.

Cuccovillo, T. & Coop, M. R. (1997). Yielding and pre-failure deformation of structured sands. *Géotechnique* **47**, No. 3, 491–508, https://doi.org/10.1680/geot.1997.47.3.491.

Dvorkin, J., Mavko, G. & Nur, A. (1991). The effect of cementation on the elastic properties of granular material. *Mech. Mater.* **12**, No. 3–4, 207–217.

Ghadir, P. & Ranjbar, N. (2018). Clayey soil stabilization using geopolymer and Portland cement. *Constr. Build. Mater.* **188**, 361–371.

Haha, M. B., Le Saout, G., Winnefeld, F. & Lothenbach, B. (2011). Influence of activator type on hydration kinetics, hydrate assemblage and microstructural development of alkali activated blast-furnace slags. *Cem. Concr. Res.* **41**, No. 3, 301–310, https://doi.org/10.1016/j.cemconres.2010.11.016.

Hancock, M. (2019). Soil mixing foundation used as an alternative to piles. *Ground Engng Mag.*. See https://www.geplus.co.

uk/news/soil-mixing-foundation-used-as-an-alternative-to-piles-12-10-2018/ (last accessed 23/05/2019).

Hird, C. & Chan, C. (2008). One-dimensional compression tests on stabilized clays incorporating shear wave velocity measurements. *Geotech. Test. J.* **31**, No. 2, 166–174.

Horpibulsuk, S., Rachan, R., Chinkulkijniwat, A., Raksachon, Y. & Suddeepong, A. (2010). Analysis of strength development in cement-stabilized silty clay from microstructural considerations. *Constr. Build. Mater.* **24**, No. 10, 2011–2021, https://doi.org/10.1016/j.conbuildmat.2010.03.011.

ICDD (International Centre for Diffraction Data) (1999). *The powder diffraction file: database of the International Centre for Diffraction Data, sets 1–49*. Newtown Square, PA, USA: ICDD.

Kang, G., Tsuchida, T. & Kim, Y. (2017). Strength and stiffness of cement-treated marine dredged clay at various curing stages. *Constr. Build. Mater.* **132**, 71–84, https://doi.org/10.1016/j.conbuildmat.2016.11.124.

Mohammadinia, A., Disfani, M. M., Conomy, D., Arulrajah, A., Horpibulsuk, S. & Darmawan, S. (2019). Utilization of alkali-activated fly ash for construction of deep mixed columns in loose sands. *J. Mater. Civ. Engng* **31**, No. 10, 04019233, https://doi.org/10.1061/(ASCE)MT.1943-5533.0002878.

Nair, S. & Little, D. N. (2009). Water as the key to expansion of ettringite in cementitious materials. *Transp. Res. Rec.* **2104**, 55–62, https://doi.org/10.3141/2104-06.

Pourakbar, S., Asadi, A., Huat, B. & Fasihnikoutalab, M. H. (2015). Soil stabilisation with alkali-activated agro-waste. *Environ. Geotech.* **2**, No. EG6, 359–370.

Rios, S., Viana da Fonseca, A. & Baudet, B. A. (2014). On the shearing behaviour of an artificially cemented soil. *Acta Geotech.* **9**, 215–226, https://doi.org/10.1007/s11440-013-0242-7.

Rios, S., Cristelo, N., Viana da Fonseca, A. & Ferreira, C. (2017). Stiffness behaviour of soil stabilized with alkali-activated fly ash from small to large strains. *Int. J. Geomech.* **17**, No. 3, 04016087, https://doi.org/10.1061/(ASCE)GM.1943-5622.0000783.

Sargent, P. (2015). *Secondary minerals to replace cement in stabilising an alluvium*. PhD thesis, Newcastle University, Newcastle upon Tyne, UK.

Sargent, P., Hughes, P. N., Rouainia, M. & White, M. L. (2013). The use of alkaline activated waste binders in enhancing the mechanical properties and durability of soft alluvial soils. *Engng Geol.* **152**, No. 1, 96–108.

Sargent, P., Hughes, P. N. & Rouainia, M. (2016). A new low carbon cementitious binder for stabilising weak ground conditions through deep soil mixing. *Soils Found. (Jpn. Geotech. Soc.)*. **56**, No. 6, 1021–1034, https://doi.org/10.1016/j.sandf.2016.11.007.

Scott, P. W., Critchley, S. R. & Wilkinson, F. C. F. (1986). The chemistry and mineralogy of some granulated and pellitized blastfurnace slags. *Mineral. Mag.* **50**, No. 355, 141–147, https://doi.org/10.1180/minmag.1986.050.355.19.

Trhlikova, J., Masin, D. & Bohac, J. (2012). Small-strain behaviour of cemented soils. *Géotechnique* **62**, No. 10, 943–947, https://doi.org/10.1680/geot.9.P.100.

Wan, H., Shui, Z. & Lin, Z. (2004). Analysis of geometric characteristics of GGBS particles and their influences on cement properties. *Cem. Concr. Res.* **34**, No. 1, 133–137, https://doi.org/10.1016/S0008-8846(03)00252-7.

Yun, T. S. & Santamarina, J. C. (2005). Decementation, softening and collapse: changes in small-strain shear stiffness in k_0 loading. *J. Geotech. Geoenviron. Engng* **131**, No. 3, 350–358.

Zhu, F., Li, Z., Dong, W. & Ou, Y. (2019). Geotechnical properties and microstructure of lime-stabilized silt clay. *Bull. Engng Geol. Environ.* **78**, No. 4, 2345–2354, https://doi.org/10.1007/s10064-018-1307-5.